AIIM

Association for Information and Image Management

1100 Wayne Avenue, Suite 1100
Silver Spring, Maryland 20910

301/587-8202

Centimeter

Inches

MANUFACTURED TO AIIM STANDARDS
BY APPLIED IMAGE, INC.

1 of 1

2

Conf-940769--7

UCRL-JC-115990
PREPRINT

Effects of Microphysics and Radiation on Mesoscale Processes of a Midlatitude Squall Line

Hung-Neng (Steve) Chin
Lawrence Livermore National Laboratory
Livermore, California 94551

Submitted to the
Tenth Conference on Numerical Weather Prediction
Portland, Oregon
July 11–12, 1994

April 1994

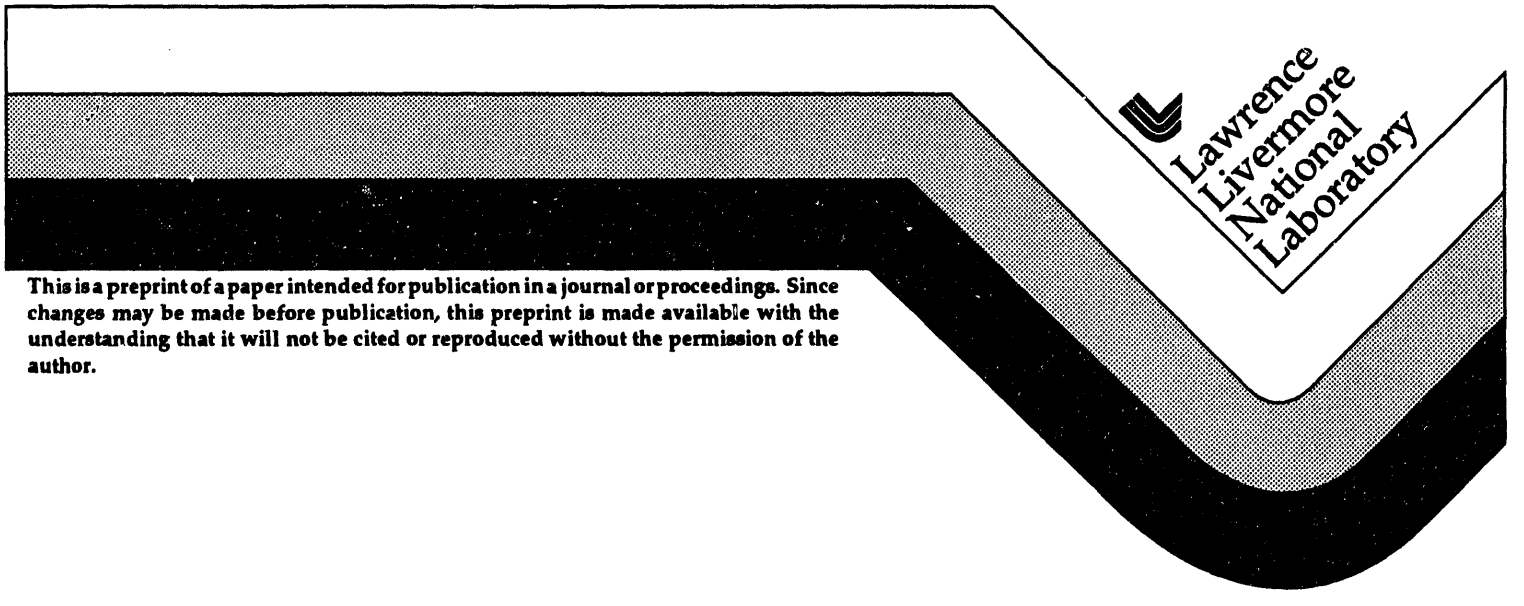

DISCLAIMER

16B.5

EFFECTS OF MICROPHYSICS AND RADIATION ON MESOSCALE PROCESSES OF A MIDLATITUDE SQUALL LINE

Hung-Neng S. Chin

Regional Atmospheric Sciences Division
Lawrence Livermore National Laboratory
Livermore, California

1. INTRODUCTION

The understanding of the essential dynamics of mesoscale convective systems (MCSs) was well addressed in the literature. Effects of different physics on mesoscale processes of MCSs are, however, not well understood at some particular aspects, such as the origins of the rear inflow and the transition zone in the radar reflectivity. The objective of this research is focused on these two aspects for a midlatitude broken-line squall system.

The existence of the rear inflow in MCSs has been identified in many observational and modeling studies (e.g., Smull and Houze, 1987; Fovell and Ogura, 1988). Although convincing evidence has shown that physical processes internal to the mesoscale system (e.g., Leary and Rappaport, 1987; Smull and Houze, 1987) and pressure gradient effects in the convective (LeMone, 1983) and trailing stratiform regions (Brown, 1979) are undoubtedly important in developing the rear inflow, it remains unclear how these internal processes interact with pressure effects to trigger the rear inflow. Moreover, many modeling studies have replicated the bright melting band (e.g., Tao *et al.*, 1993), but the transition zone has not been successfully simulated. With the enhanced model physics, such as radiation, in a cloud model (Chin, 1993), we can simulate these features and provide some supplemental evidences, at least in part, to explain them. The modulation of the rear inflow by microphysics, long- (LW) and shortwave (SW) radiation, and its related cloud-radiative feedback to the modeled squall line system are also discussed in this study.

2. MODEL AND INITIALIZATION

The model used is an extension of Chin and Ogura's (1989) two-dimensional cloud model; major improvements include ice microphysics, radiation and their computational efficiency. The modified parameterizations of ice microphysics and radiation are able to simulate MCSs with a prominent anvil and to distinguish the phase impact of hydrometeors on the cloud optical properties (Chin, 1993). The model is nonhydrostatic and compressible. Physical modules include an upper-level sponge damping layer, a planetary boundary layer parameterization, turbulence, a two-category liquid water scheme (cloud droplet and raindrop), a three-category ice-phase scheme (ice crystal, snow and hail), and LW and SW radiation. The Coriolis force is ignored in this study to avoid the complication with the LW cloud-top cooling effect on trapping gravity waves (Tripoli and Cotton, 1989b).

Surface temperature and moisture in this study are fixed to eliminate the possible influence of surface conditions on the cloud-radiation interactions. Open boundary conditions are applied at the lateral boundaries. A rigid boundary condition is imposed at upper and lower boundaries, with a sponge damping layer placed above 15 km to minimize the reflection of internal gravity waves from the rigid upper boundary. The Galilean transformation is adopted to keep the modeled squall line system within the central portion of model domain. A time filter is also used to control the computational instability of the leapfrog scheme.

Simulations without the ice-phase scheme (referred as ice-free runs) and simulations with both liquid and ice water schemes (ice runs) are performed in two sets of experiments. Each set (ice-free or ice) consists of three model runs: a control run (without radiation), a simulation with LW radiation only, and one with both LW and SW radiation. A total of six runs are shown in this study. All simulations are integrated for eight hours of physical time to reach a quasi-equilibrium stage. For the experiment with SW radiation, the local time between 0800 and 1600 LST was chosen.

The initial conditions are based on a composite sounding (Bluestein and Jain, 1985) with modified temperature and moisture profiles to represent a mixed layer below 800 mb, as being often observed in pre-storm conditions at midlatitudes. The base state wind (normal to the squall line) of the composite sounding increased nearly linearly with height from the surface to 8 km. Above 8 km, the wind is modified to have a jet profile below 10 km and a constant profile above 10 km. The convective available potential energy and bulk Richardson number of the initial conditions are 2742 J kg^{-1} and 74.4, respectively. The model is

Corresponding author address: Dr. H.-N. S. Chin, P.O. Box 808 (L-262), Livermore, CA 94551.

initialized by a warm, moist bubble and a horizontally homogeneous sounding. This bubble is 20 km wide and 3 km deep, and is centered at 1.5 km above the ground. Maximum perturbations of potential temperature and the mixing ratio of water vapor are 2 K and 2 g kg^{-1}, respectively.

3. RESULTS

a. Origin of Rear Inflow

The time-averaged dynamic structure at the mature stage of both ice-free and ice control runs indicates that the simulated storm is organized in a multicellular mode (not shown); these features include the upshear (west) tilt of convective cores, decaying convection located at the upshear side of developed deep convection, strong easterly flow in the region of upward motion, returning upper-level westerly outflow within the leading anvil, and mid- to low-level strong rear inflow behind the leading edge with a returning outflow underneath. Both control runs also show a strong rear inflow with the maximum over 10 m s^{-1} (see Table 1). A significant difference in the dynamic structure between the initial stage and the mature state is the upshear tilt (to west) of convective cores.

To validate the previous speculation on the mechanism that causes the development of the rear inflow (Smull and Houze, 1987), temporally averaged structures at the earlier stages of ice-free control run are used (Fig 1a-d). While the convective core remains nearly upright, there is weak westerly flow in response to a weak low pressure perturbation and it is confined in a small area at mid-levels behind the convective region (Fig. 1a-b). Later, a wide rearward expansion of the low pressure zone along with pronounced upshear (west) tilt of convective cores (Fig. 1c-d) coincides with the occurrence of the strongest cold pool intensity (not shown) and the rapid deepening of low pressure minimum (from -2.7 to -4.9 mb). The decomposed pressure perturbation indicates that this pressure minimum is primarily contributed by the buoyancy term (over 90%). This result is consistent with LeMone's (1983) finding, where the hydrostatically-induced pressure perturbation was attributed to the warming aloft in rearward-sloping deep towers. Thus, the enhanced pressure force intensifies the horizontal wind field and result in the development of rear inflow.

The observed descending rear inflow is also simulated as a result of the strong evaporative cooling of rain water due to the merging with the convective downdraft behind the system's leading edge. The interaction of penetrating rear inflow with low-level incoming flow also indicates the influence of rear inflow on the convective activity near the leading edge. As the system ages to the mature stage, the sloping rear inflow and easterly flow above further expand rearward and result in a deepening of the low pressure zone in the stratiform region. The deepening of this hydrostatically-induced meso-low is supported by Brown's (1979) finding and results from latent heating above melting and evaporative cooling. Once convective cores significantly tilt rearward, the variation of pressure minimum becomes small as the system evolves into the mature stage. Similar results are also found in the ice control run (not shown).

On the whole, model results indicate that the intensification of the low pressure perturbation and development of the rear inflow is triggered by microphysical processes, mainly the evaporation of rain water (and sublimation of snow and hail if the ice phase is included) at mid- and low-levels of the convective region. This overwhelming cooling interacts with the vertical wind shear and leads to the upshear tilt of convective cores. The chain reactions of the rearward tilt of convective cores, then, develop the well-known mesoscale features. This finding supports the previous speculation on the mechanism that generates the rear inflow.

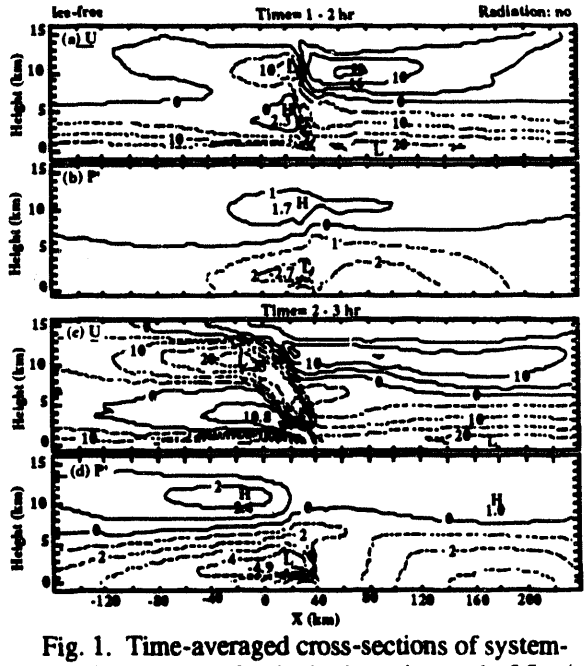

Fig. 1. Time-averaged cross-sections of system-relative horizontal velocity in an interval of 5 m/s and pressure perturbation with the contour of 1 mb for the ice-free control run. (a)-(b) between 1 and 2 hours. (c)-(d) between 2 and 3 hours.

b. Ice phase and Radiation Impact on Rear Inflow

The rear inflow is an interesting and controversial phenomenon of MCSs. Zhang and Gao (1989) speculated that this inflow may aid or impede the storm, depending on the environmental conditions while the observations (e.g., Smull and Houze, 1987) support the hypothesis that the strong rear inflow enhances the convective portion of the storm. To investigate this phenomenon, time-averaged statistics of the rear inflow maximum and the hydrostatically-

induced pressure minimum at the mature stage of the modeled squall line system are used (Table 1). Both ice-free and ice simulations show a consistent variation of the rear inflow with LW and SW radiation; these results indicate that LW radiation results in a stronger rear inflow jet, that is weakened as SW radiation is included. However, the pressure perturbation shows an inverse correlation with LW and SW radiation.

As shown in the control runs, the ice phase weakens the rear inflow jet and intensifies the low pressure minimum. Therefore, the horizontal pressure force cannot explain the changes in the rear inflow caused by the ice phase. The collocation of the rear inflow maximum and the low pressure minimum in the convective region (see Fig. 1c-d), however, suggests a close relation between reduced low-level convective precipitation and weaker rear inflow in the ice control run. Since evaporative cooling is enhanced in the convective region of ice control run, this cooling seems not to be the cause of a weaker convective downdraft. As indicated in the water budget (not shown), more water mass in the ice control run is transported into the stratiform region mainly due to the smaller fall speed of snowflakes than that of rain water in the ice-free case. Therefore, it is most likely that the weaker convective downdraft underneath the sloping convective towers in the ice control run is caused by the reduced low-level water-loading. The smaller convective downdraft of ice control run, thus, produces a weaker rear inflow through mass continuity as the induced horizontal flow approaches the convective region from behind.

To further examine the reverse relationship of rear inflow and pressure perturbation with microphysics, the decomposed pressure fields from the temporally averaged structure of both control runs are used (not shown). The pressure perturbation is decomposed into drag, wind deformation and buoyancy terms (Wilhelmson and Ogura, 1972). Results indicate that the buoyancy terms in both control runs account for more than 90% of the total pressure perturbation minimum. The drag term contributes only a small portion to the pressure minimum (< 4%). The wind deformation term weakens the pressure minimum although its magnitude (< 10%) is much smaller than that of the buoyancy term. Since the magnitudes of buoyancy and wind deformation terms are related to the temperature-moisture structure and the induced rear inflow, the colder and drier low-level structure and the weaker rear inflow in the ice control run produces a more intense pressure minimum than its ice-free counterpart.

In addition to microphysics, the pressure minimum and the rear inflow maximum is also modulated by radiation. As shown in Tables 1 and 2, LW/SW radiation weakens/enhances the hydrostatically-induced pressure minimum, but enhances/weakens the convective activity. The variation of the pressure minimum is, therefore, most likely the consequence of change in the rear inflow. The enhanced/reduced precipitation by LW/SW radiation can result in a stronger/weaker downdraft, that intensifies/weakens the rear inflow through mass continuity. Therefore, simulations with LW/SW radiation reveal that the increased/decreased rear inflow magnifies/weakens the wind deformation, and results in a weaker/stronger pressure minimum.

Table 1. Intensities of the rear inflow and pressure perturbation during the mature stage.

Microphysics	ice-free			ice		
Radiation	no	LW	LW + SW	no	LW	LW + SW
Rear Inflow Jet (m s^{-1})	12.4	13.2	11.5	10.2	11.1	10.2
P'_{min} (mb)	-5.4	-5.0	-5.5	-6.0	-5.4	-5.9

Table 2. Normalized total mass of the precipitating water during the mature stage.

Microphysics	ice-free			ice		
Radiation	no * (4.42)	LW	LW+SW	no (9.21)*	LW	LW+SW
Convective	85.7%	86.6%	82.5%	66.8%	68.9%	63.9%
Stratiform	14.3%	15.3%	14.5%	33.2%	36.7%	34.5%

* the number in parenthesis is the total mass of control runs in (x 10^4) kg / m.

c. Radiation Impact on Microphysical Structure

Besides the impact on the rear inflow, both the ice phase and radiation also play an important role in modulating the mesoscale structure of the modeled squall line system. As shown in Fig. 2a, the addition of the ice phase leads to a substantial amount of stratiform precipitation spreading over a wider area (mainly in the form of snowflakes due to their small fall speed) and having a pronounced band near the freezing level as a result of the melting of ice particles. This feature is not found in the ice-free run. However, the transition zone is not simulated in the ice control run unless LW radiation is included (Fig. 2b). Due to both the vertical trapping of gravity waves (Tripoli and Cotton, 1989b) and the intensified deep convection (Table 2), the enhanced mesoscale circulation (not shown) by LW radiation causes a separation between the bright melting band and the convective region. The addition of LW radiation produces a stronger upper outflow (above the transition zone) during the mature stage (in 3 hours) than its counterpart in the control run by ~ 5 m s^{-1}. This enhanced rearward outflow allows the hydrometeors to move further west by 54 km, that is comparable to the distance between the bright melting band and the convective region (see Fig. 2b). This spatial scale match provides convincing evidence to support the hypothesis that the transition zone is caused by LW radiation. This structure becomes less distinct when SW radiation weakens the mesoscale circulation (not shown).

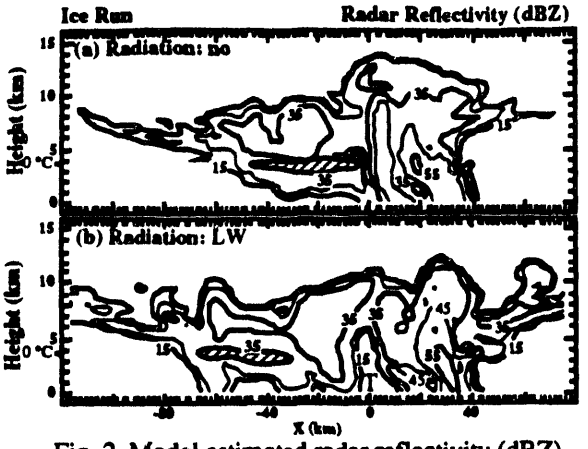

Fig. 2. Model estimated radar reflectivity (dBZ) near time = 8 hour of ice simulations. (a) control run. (b) with only longwave (LW) radiation. The contour interval is 10 dBZ. Shading regions represent the bright melting bands and T marks the location of transition zone.

4. CONCLUSIONS

The simulated squall line systems are organized in the multicellular behavior, as observed in real storms. Results show that although both the ice phase and radiation have little influence on the multicellular characters of the modeled squall line system, a realistic mesoscale structure with a transition zone between the bright melting band and the convective region is simulated as a result of both small fall velocity of snowflakes and the intensified mesoscale circulation by LW radiation. The coincidence of the development of rear inflow with tilting convective cores supports the earlier speculation on the origin of rear inflow. Results also indicate that this rear inflow results from the rapid deepening of the hydrostatically-induced low pressure associated with sloping deep convection.

Both ice-free and ice simulations also show that radiation has a impact on the rear inflow, stratiform clouds and convective activity. In addition, the negative correlation of water content between stratiform clouds and the upper part of the convective region suggests that radiation does not directly affect overall convective activity. Instead, radiation directly impacts the stratiform cloud; the resulting stratiform downdraft alters the intensity of the rear inflow through mass continuity. The enhanced/weakened rear inflow by LW/SW radiation further interacts with the convective portion of the modeled squall line system, and results in stronger/weaker transport of hydrometeors into the stratiform cloud due to the enhanced/weakened convective activity. This transport further impacts stratiform precipitation and downdraft. The chain reaction is, thus, triggered between stratiform and convective regions. As a whole, LW/SW radiation exhibits positive/negative feedback to the modeled squall line system through the enhanced/weakened rear inflow as a result of the scale interaction between stratiform and convective regions.

ACKNOWLEDGMENTS. This work was supported by the Department of Energy (DOE) ARM[1] program and conducted under the auspices of the U. S. DOE by the Lawrence Livermore National Laboratory under contract No. W-7405-ENG-48.

REFERENCES:

Bluestein, H. B., and M. H. Jain, 1985: Formation of mesoscale lines of precipitation: Severe squall lines in Oklahoma during the spring. *J. Atmos. Sci.*, **42**, 1711-1732.

Brown, J. M., 1979: Mesoscale unsaturated downdrafts driven by rainfall evaporation: A numerical study. *J. Atmos. Sci.*, **36**, 313-338.

Chin, H.-N. S., and Y. Ogura, 1989: Supplementary modeling study of a tropical convective band. *J. Atmos. Sci.*, **46**, 1440-1447.

Chin, H.-N. S., 1993: The impact of the ice phase and radiation on a midlatitude squall line. (submitted to *J. Atmos. Sci.*, in final review)

Fovell, R. G., and Y. Ogura, 1988: Numerical simulation of a midlatitude squall line in two dimensions. *J. Atmos. Sci.*, **45**, 3846-3879.

Leary, C. A., and E. N. Rappaport, 1987: The life cycle and internal structure of a mesoscale convective complex. *Mon. Wea. Rev.*, **115**, 1503-1527.

LeMone, M. A., 1983: Momentum transport by a line of cumulo-nimbus. *J. Atmos. Sci.*, **40**, 1815-1834.

Smull, B., and R. A. Houze, Jr., 1987: Rear inflow in squall lines with trailing stratiform precipitation. *Mon. Wea. Rev.*, **115**, 2869-2889.

Tao, W.-K., J. Simpson, C.-H. Sui, B. Ferrier, S. Lang, J. Scala, M.-D. Chou, and K. Pickering, 1993: Heating, moisture and water budgets of tropical and midlatitude squall lines: Comparisons and sensitivity to longwave radiation. *J. Atmos. Sci.*, **50**, 673-690.

Tripoli, G. J., and W. R. Cotton, 1989b: Numerical Study of an Observed Orogenic Mesoscale Convective System. Part 2: Analysis of Governing Dynamics. *Mon. Wea. Rev.*, **117**, 305-328.

Wilheimson, R. B., and Y. Ogura, 1972: The pressure perturbation and the numerical modeling of a cloud. *J. Atmos. Sci.*, **29**, 1295-1307.

Zhang, D.-L., and K. Gao, 1989: Numerical simulation of an intense squall line during 10-11 June 1985 PRE-STORM. Part II: Rear inflow, surface pressure perturbations and stratiform precipitation. *Mon. Wea. Rev.*, **117**, 2067-2094.

[1] Atmospheric Radiation Measurement

DATE
FILMED
9/23/94
END